



Using Confocal Laser Scanning Microscopy to Analyze the Mass Transfer in the Protein A Medium of a Silica Matrix

Katsuda, Tomohisa
Yamaguchi, Tomoki
Kase, Yuki
Ota, Kou
Yamaji, Hideki

(Citation)

Journal of Chemical Engineering of Japan, 56(1):2179369

(Issue Date)

2023-12-31

(Resource Type)

journal article

(Version)

Version of Record

(Rights)

© 2023 The Author(s). Published with license by Taylor & Francis Group, LLC
This is an Open Access article distributed under the terms of the Creative Commons Attribution License (<http://creativecommons.org/licenses/by/4.0/>), which permits unrestricted use, distribution, and reproduction in any medium, provided the original work is properly cited.

(URL)

<https://hdl.handle.net/20.500.14094/0100482052>



Using Confocal Laser Scanning Microscopy to Analyze the Mass Transfer in the Protein A Medium of a Silica Matrix

Tomohisa Katsuda, Tomoki Yamaguchi, Yuki Kase, Kou Ota & Hideki Yamaji

To cite this article: Tomohisa Katsuda, Tomoki Yamaguchi, Yuki Kase, Kou Ota & Hideki Yamaji (2023) Using Confocal Laser Scanning Microscopy to Analyze the Mass Transfer in the Protein A Medium of a Silica Matrix, *Journal of Chemical Engineering of Japan*, 56:1, 2179369, DOI: 10.1080/00219592.2023.2179369

To link to this article: <https://doi.org/10.1080/00219592.2023.2179369>



© 2023 The Author(s). Published with
license by Taylor & Francis Group, LLC



[View supplementary material](#)



Published online: 22 Feb 2023.



Submit your article to this journal 



Article views: 171



[View related articles](#) 

View Crossmark data

Using Confocal Laser Scanning Microscopy to Analyze the Mass Transfer in the Protein A Medium of a Silica Matrix

Tomohisa Katsuda, Tomoki Yamaguchi, Yuki Kase, Kou Ota, and Hideki Yamaji

Department of Chemical Science and Engineering, Graduate School of Engineering, Kobe University, 1-1 Rokkodai-cho, Nada-ku, Kobe-shi, Hyogo 657-8501, Japan

ABSTRACT

Mass transfer in a protein A medium with a silica matrix was analyzed in this study. Using confocal laser scanning microscopy, we monitored the positional and temporal changes in the polyclonal human IgG during batch adsorption. A simple theoretical model based on Fick's law of diffusion and Langmuir adsorption was used to numerically approximate the external and intraparticle mass-transfer properties of IgG in single particles. The diffusivities found in this study were validated by comparing with the values reported in other studies and also by using numerical calculation to reproduce the experimentally obtained breakthrough curve.

ARTICLE HISTORY

Received 15 May 2022
Revised 23 January 2023
Accepted 8 February 2023

KEYWORDS

Protein A medium; Confocal laser scanning microscopy; Mass transfer; Apparent diffusivity; Finite difference method


1. Introduction


Affinity-chromatography media harnessing Staphylococcal protein A, or its derivatives, have generally been used in the downstream processing of monoclonal antibody drugs due to their highly selective binding with immunoglobulin G (IgG). Such protein A media consist mostly of matrices that are spherical and either porous or highly cross-linked. IgG is a protein with a relatively large molecular mass of approximately 150 kDa and a low diffusivity in aqueous solutions of approximately $4 \times 10^{-11} \text{ m}^2 \cdot \text{s}^{-1}$ (Jøssang et al. 1988). Thus, the nature of IgG has raised concerns about their mass transfer in protein A media.

External and intraparticle mass transfers are known to affect the adsorption rate of a medium and the dynamic binding capacity (DBC) of a packed column and are traditionally quantified using film mass-transfer coefficients and effective diffusivities, respectively (Horstmann and Chase 1989). These values are conventionally determined by measuring the adsorbate concentration in the continuous phase (outside particles) during the course of adsorption (Armenante and Kirwan 1989; Horstmann and Chase 1989; Hahn et al. 2005; Tscheliessnig et al. 2005). Microscopic methods based on the direct observation of uptake in a particle, on the other hand, have also been conducted (Subramanian et al. 1994; Kim et al. 1996; Hubbuch et al. 2002; Stone and Carta 2007).

Since the mid-1990s confocal laser scanning microscopy (CLSM) has been used to visualize the adsorption process

within a particle (Kim et al. 1996; Ljunglöf and Hjorth 1996). CLSM is an enhancement of epifluorescence microscopy. The microscope equipped with a confocal optical system is able to optically section a fluorescently-stained specimen with each focal plane. In the subsequent decades the quantitative analysis of mass transfer using CLSM was established (Kasche et al. 2003; Zhou et al. 2006; Schröder et al. 2006; Susanto et al. 2007; Bowes and Lenhoff 2011). These studies and determinations were focused mostly on ion exchangers owing to their wide range of applications and also to satisfy scientific interest by clarifying a complicated adsorption mechanism that involves both diffusion and electrostatic interaction (Yamamoto et al. 1988; LeVan et al. 1999). In contrast to ion exchangers, we did not anticipate the scarcity of reports on affinity media with an adsorption mechanism that is dependent on the selective interaction between ligands and adsorbate molecules (Ljunglöf and Hjorth 1996; Ljunglöf and Thömmes 1998; Linden et al. 1999; Linden et al. 2002; Sheth 2009; Weinberg et al. 2017). Because of the simplicity of the adsorption mechanism in affinity media, however, characteristics of the matrix structure such as pore size, porosity, tortuosity, etc., may have a more significant role in the adsorption behavior, particularly in protein A media. It would be useful to represent these matrix features in association with the mass-transfer properties that could allow a comparison of media and/or a scale-up of packed columns. This could benefit both manufacturers and customers of protein A media.

CONTACT Tomohisa Katsuda  katsuda@kobe-u.ac.jp

 Supplemental data for this article can be accessed online at <https://doi.org/10.1080/00219592.2023.2179369>

© 2023 The Author(s). Published with license by Taylor & Francis Group, LLC

This is an Open Access article distributed under the terms of the Creative Commons Attribution License (<http://creativecommons.org/licenses/by/4.0/>), which permits unrestricted use, distribution, and reproduction in any medium, provided the original work is properly cited.

In this study, we analyzed the mass transfer of IgG in a silica-based protein A medium with an optimized pore size (Katoh et al. 2007; Miyahara et al. 2012). In order to determine the apparent diffusivities of IgG in the protein A medium, the positional and temporal changes in the adsorption amount observed via CLSM in single particles were approximated using a simple theoretical model based on both Fick's law of diffusion and the Langmuir adsorption model.

2. Experimental

2.1. Materials

The two media used in this study included a silica-based protein A medium, M.S.Gel Protein A-D-50-1000AW (Katoh et al. 2007; Miyahara et al. 2012), which was kindly provided by AGC Si-Tech Co., Ltd. (Kitakyushu, Japan), and a cross-linked agarose-based medium, MabSelect Xtra, that was obtained from Cytiva (Tokyo, Japan). The dispersion medium for storage was replaced with phosphate-buffered saline (PBS) just before use via resuspending 3 times. We purchased "IgG from human serum" (I4506, Sigma-Aldrich) and "IgG-FITC from human serum" (F9636, *ditto*) for use as a polyclonal human IgG (hIgG) and a fluorescein-isothiocyanate conjugate (FITC-hIgG), respectively. A lyophilized powder of hIgG was reconstituted with PBS according to the manufacturer's information. The molar ratio of fluorescent dye to protein (F/P molar ratio) of the FITC-hIgG we used was initially 2.4. The use of FITC-hIgG was avoided when the F/P molar ratio was found to have decreased to less than 1.5. The F/P molar ratios were determined spectrophotometrically (UV-1900, Shimadzu, Kyoto, Japan) based on both A_{280} and A_{494} (Thermo Fisher Scientific Inc. 2011). The PBS that was used consisted of 137 mM NaCl ($8 \text{ g}\cdot\text{L}^{-1}$), 2.7 mM KCl ($0.2 \text{ g}\cdot\text{L}^{-1}$), 8.4 mM $\text{Na}_2\text{HPO}_4\cdot 12\text{H}_2\text{O}$ ($3 \text{ g}\cdot\text{L}^{-1}$), and 1.5 mM KH_2PO_4 ($0.2 \text{ g}\cdot\text{L}^{-1}$); it was adjusted to a pH of 7.4 and subsequently filtered using a $0.2 \mu\text{m}$ polyethersulfone filter (596-3320, Nalgene). All chemicals used in this study were of reagent grade.

2.2. Batch adsorption for isotherm

We prepared hIgG solutions ranging from 0 to $1 \text{ mg}\cdot\text{mL}^{-1}$ with PBS, and 1 mL of each solution was placed in a 2 mL low-protein-binding microtube (PK-20C-500, Watson). The resuspended slurry of a protein A medium equivalent to $6 \mu\text{L}$ in a packed-bed volume was added to each microtube and mixed overnight using a rotating mixer (RT-50, Taitec; 16 rpm) at room temperature. The supernatant was obtained from each microtube via centrifugation at $480 \times g$ for several seconds, and the concentrations of free hIgG were determined spectrophotometrically based on A_{280} . For this spectrophotometric measurement we predetermined that the initial concentration would be at least $0.2 \text{ mg}\cdot\text{mL}^{-1}$ in order to ensure that an equilibrium concentration would result in a reliable absorbance of ≥ 0.005 . We considered this free-hIgG concentration to be the equilibrium value, c^*

$[\text{mg}\cdot\text{mL}^{-1}\text{-liquid}]$, and the equilibrium adsorption amounts of hIgG per packed-bed volume, q_b^* $[\text{mg}\cdot\text{mL}^{-1}\text{-packed-bed}]$, were determined by dividing each difference between the initial and the determined concentrations of free hIgG by the packed-bed volume of the protein A medium that was added ($6 \mu\text{L}$). The maximum amount of adsorption per packed-bed volume, q_{bm} $[\text{mg}\cdot\text{mL}^{-1}\text{-packed-bed}]$, and the dissociation constant between protein A and hIgG, K_d $[\text{mg}\cdot\text{mL}^{-1}\text{-liquid}]$ were determined based on the Langmuir adsorption isotherm (Langmuir 1916), which is expressed here as Eq. (1).

$$q_b^* = \frac{q_{bm}c^*}{K_d + c^*} \quad (1)$$

2.3. Batch adsorption for the observation of adsorption behavior

In order to assume the free hIgG concentration in the continuous phase would remain constant during batch adsorption, an excess amount of hIgG was supplied to the protein A medium: 13.9 mg of hIgG was dissolved in 694 mL of PBS together with 3.47 mg of FITC-hIgG, and then $10 \mu\text{L}$ in a packed-bed volume of the protein A medium was added. When total 17.4 mg of IgG was used, it corresponded to 24-fold the maximum adsorption amount by the protein A medium in the suspension and resulted in a hIgG concentration of $0.025 \text{ mg}\cdot\text{mL}^{-1}$. At a FITC-hIgG concentration of $0.005 \text{ mg}\cdot\text{mL}^{-1}$, the fluorescence of the solution was negligible (substantially undetectable), but that of the adsorbing particle was detectable. This mixture was placed in a 1,000 mL laboratory glass bottle (a nominal outside diameter of 101 mm), and ambient light was blocked with aluminum foil. The mixture was then agitated with a magnetic stirrer at 300 rpm. In this bottle a 694 mL hIgG solution showed a liquid height of 102 mm and an internal diameter of 93 mm. A magnetic-stirrer bar with a round-rod shape (50 mm in length and 7.5 mm in diameter) was used and held 20 mm above the bottom of the bottle by hanging from the top using a stainless-steel wire and a swivel that would prevent the protein A medium from being ground. The adsorption was carried out at room temperature.

A small portion of the mixture (2 mL) was occasionally sampled. The protein A medium in the mixture was sedimented by centrifugation at $480 \times g$ for several seconds, washed once with PBS, and then concentrated by resuspension in $200 \mu\text{L}$ PBS. This resuspension was immediately frozen in liquid nitrogen to conserve the state of adsorption within a particle and kept frozen until microscopic observation.

2.4. CLSM observation of intraparticle adsorption behavior

We used a confocal laser scanning microscope (FV1000, Olympus), which was equipped with an Ar laser (30 mW) and an inverted microscope. The filters and the dichroic mirrors employed were for FICT, and the excitation and

emission wavelengths were at 488 and 519 nm, respectively. The objective lens used for observations featured 40 \times magnification and a numerical aperture of 0.95 (UPLSAPO 40 \times 2, Olympus). A confocal aperture of 100 μm was selected. These optical settings provided optical resolutions of 0.248 μm /pixel horizontally and 0.5 μm /slice vertically. To maintain the sensitivity of the photomultiplier tube in the microscope during observations, we chose a “photon-counting” mode that would be suitable for the detection of weak light, and the excitation laser transmission was adjusted to 1.0%.

A frozen sample of the protein A medium was thawed just before observation and a drop of the suspension was placed on a hemocytometer with a depth of 0.1 mm (Thoma, Sunlead Glass). We used a hemocytometer to prevent distortions such as flattening of the particles, and we used a cover glass with a thickness of 0.11–0.23 mm, which was suitable for the objective lens. The microscope was focused to sharpen the outline of adsorbent particles and then cross-sectional images were taken by scanning a 127 \times 127 μm area horizontally and \pm 5 μm vertically. The scanning speed was 12.5 μs /pixel. The cross-sectional image with the largest particle diameter was considered to be that of the plane passing through the center of the particle. In reference to this image we obtained the distribution of fluorescence intensities along a line passing through the particle center and assumed it represented the local adsorption amounts of hIgG in the particle. Such a distribution was obtained for at least 3 particles in each sample and analyzed in the manner described in the following section.

2.5. Fixed-bed adsorption

To obtain an example of breakthrough curves we performed a fixed-bed adsorption of hIgG by the silica-based protein A medium packed in a Tricorn 5/50 column (Cytiva) at a bed height of 30 mm. Using ÄKTAprius plus (Cytiva), we maintained the flow rate in the column at 0.6 mL \cdot min $^{-1}$ and continuously monitored A_{280} of a flow-through. After equilibration with 10 column volumes of PBS, 0.4 mg \cdot mL $^{-1}$ of hIgG solution was loaded until the absorbance ceased to increase.

3. Analyses

3.1. Conversion of the fluorescence intensities of local adsorption amounts of hIgG

The distribution of fluorescence intensities was smoothed using a simple moving-average method of gathering five consecutive examples of raw data from each side of every data point (Figure 1). Considering the fluorescence intensities within a particle increase along the adsorption, the coordinates of the outer particle surfaces were determined from both edges of this high-intensity region. The middle of these coordinates was considered to be the center of the particle, and the distance from the center, r [m], was normalized to the particle radius, R [m]. Then the fluorescence

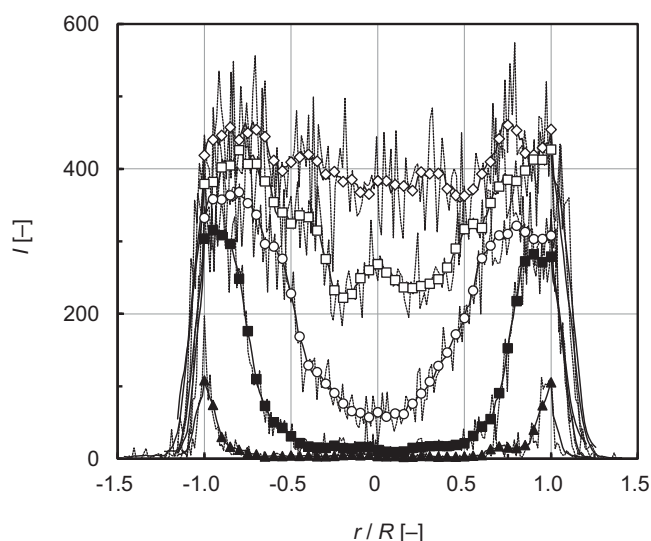


Figure 1. Distributions of the fluorescence intensities measured in single particles of the silica-based protein A medium. The dotted lines show raw data obtained from a representative particle for each adsorption time and the solid ones are the curves smoothed with a simple moving-average method. Keys: closed triangles, adsorption time of 1 h; closed squares, 2 h; open circles, 4 h; open squares, 8 h; and, open diamonds, 28 h.

intensities at predetermined normalized distances (r/R) were determined via linear interpolation between the nearest two data points followed by determining the average among the particles of each sample. The sample of 28-h adsorption was considered to be in equilibrium, and a conversion factor that related fluorescence intensity to an adsorption amount was determined by dividing the equilibrium adsorption amount by the fluorescence intensity integrated over the entire particle, as per Eq. (2).

$$\alpha = \frac{q_b^*}{\sum \frac{r_{i+1}^3 - r_i^3}{R^3} I_{r_i}^*} \quad (2)$$

Here, α is the conversion factor [mg \cdot mL $^{-1}$ -packed-bed] and $I_{r_i}^*$ is the fluorescence intensity in equilibrium (arbitrary unit) at distance r . The subscript i is the index of the data-points numbered from the center to the outer surface. Using this conversion factor, we determined the local adsorption amounts of each sample from the fluorescence intensities in CLSM.

3.2. Numerical approximation of the local adsorption amounts

The local adsorption amounts were approximated with the numerical solution of a simple theoretical model representing both external and intraparticle mass transfers and adsorption. For consistency, we applied Fick's law of diffusion to both of the mass transfers, but allowed discontinuity in the apparent diffusivities between the interior and the surface of the particle. Also, the matrix structure could differ according to position within a particle. Consequently, we assumed the apparent diffusivities would vary according to the distance from the center in addition to differences between the particle interior and the surface. On the other hand, the rates of adsorption and desorption shown in the

kinetic derivation of the Langmuir adsorption model (Langmuir 1916; Chase 1984) were applied to express the adsorption behavior.

Particles are assumed to have concentric spherical shells with a thickness designated as Δr [m]. By considering the mass balance in the intraparticle liquid phase of a shell according to the distance from the center, r , within a short time from t to $t + \Delta t$, the concentration of free hIgG, c [$\text{mol} \cdot \text{m}^{-3}$], and the amount of adsorbed hIgG per pore volume (the volume of the intraparticle liquid phase), q [$\text{mol} \cdot \text{m}^{-3}$], can then be expressed in finite-difference form, as shown by Eqs. (3) and (4).

$$c_r^{t+\Delta t} = c_r^t + \frac{D'_{e,r}\Delta t}{\Delta r^2} (c_{r+\Delta r}^t - c_r^t) - \frac{D'_{e,r-\Delta r}\Delta t}{\Delta r^2} \left(\frac{r-\Delta r}{r}\right)^2 (c_r^t - c_{r-\Delta r}^t) - k_a\Delta t \{c_r^t(q_{m,r} - q_r^t) - K_d q_r^t\} \quad (3)$$

$$q_r^{t+\Delta t} = q_r^t + k_a\Delta t \{c_r^t(q_{m,r} - q_r^t) - K_d q_r^t\} \quad (4)$$

In Eqs. (3) and (4), D'_e is the apparent diffusivity [$\text{m}^2 \cdot \text{s}^{-1}$], q_m is the maximum amount of adsorbed hIgG per pore volume [$\text{mol} \cdot \text{m}^{-3}$], k_a is the association rate constant [$\text{m}^3 \cdot \text{mol}^{-1} \cdot \text{s}^{-1}$], and K_d is the dissociation constant [$\text{mol} \cdot \text{m}^{-3}$]. The above concentrations and adsorption amounts in the concentric spherical shells are illustrated in Figure 2.

Since it was being applied particularly to the concentration gradient within pores, the apparent diffusivity in this study, D'_e , was distinguished from the general effective diffusivity, D_e , as shown by Eq. (5).

$$D_e \left(= \frac{\varepsilon_p}{\tau} D_m \right) = \varepsilon_p D'_e \quad (5)$$

In Eq. (5), ε_p is the porosity of adsorbent particles, τ is the tortuosity factor [-], and D_m is the molecular diffusivity [$\text{m}^2 \cdot \text{s}^{-1}$]. In this context, the film mass-transfer coefficient, k_f , is usually defined in reference to a homogeneous (non-porous) boundary, and is therefore expressed by the apparent diffusivity of the particle surface, $D'_{e,R}$, as shown by Eq. (6).

$$k_f \left(= \frac{D_m}{\delta} \right) = \frac{D'_{e,R}}{\Delta r} \quad (6)$$

In Eq. (6), δ is the film thickness [m]. On the other hand, the adsorption amount per pore volume, q , in these equations was obtained from the adsorption amount per packed-bed volume, q_b , by using Eq. (7).

$$q = \frac{q_b}{(1 - \varepsilon)\varepsilon_p} \quad (7)$$

In Eq. (7), ε is the void fraction of the packed bed.

By using the dimensionless concentration, C ($= c/c_0$), and the adsorption ratio, Q ($= q/q_m$), Eqs. (3) and (4) were transformed as shown by Eqs. (8) and (9).

$$C_r^{t+\Delta t} = C_r^t + \frac{D'_{e,r}\Delta t}{\Delta r^2} (C_{r+\Delta r}^t - C_r^t) - \frac{D'_{e,r-\Delta r}\Delta t}{\Delta r^2} \left(\frac{r-\Delta r}{r}\right)^2 (C_r^t - C_{r-\Delta r}^t) - k_a q_{m,r} \Delta t \left\{ C_r^t (1 - Q_r^t) - \frac{K_d}{c_0} Q_r^t \right\} \quad (8)$$

$$Q_r^{t+\Delta t} = Q_r^t + k_a c_0 \Delta t \left\{ C_r^t (1 - Q_r^t) - \frac{K_d}{c_0} Q_r^t \right\} \quad (9)$$

In Eqs. (8) and (9), c_0 is the concentration of hIgG in the continuous phase [$\text{mol} \cdot \text{m}^{-3}$]. The initial and boundary conditions were applied to Eqs. (8) and (9), as shown by Eqs. (10)–(13).

$$C_r^0 = 0, \quad 0 \leq r \leq R \quad (10)$$

$$Q_r^0 = 0, \quad 0 \leq r \leq R \quad (11)$$

$$C_{R+\Delta r}^t = 1, \quad t \geq 0 \quad (12)$$

$$C_0^t = C_{\Delta r}^t, \quad t \geq 0 \quad (13)$$

In Eqs. (10)–(13), $r=R$ and $R+\Delta r$ correspond to the outermost shell and the continuous phase, respectively. Eqs. (8)–(13) were solved with an explicit numerical method using the software Microsoft Visual Basic for Applications in Excel. Through a trial-and-error approach we determined the apparent diffusivities that would best approximate the adsorption ratios obtained from CLSM with the above numerical calculations.

3.3. Numerical calculation of breakthrough curves

The concentration of IgG in a fixed-bed column was expressed by a finite-difference equation that accounted for advection, axial dispersion, and adsorption, and this was solved explicitly to obtain the breakthrough curves. By assuming thin cross-sections with the thickness, Δl [m], in the direction of the axial length, L [m], of a column, we obtained the mass balance in the mobile phase of the cross-sections at a distance from the column inlet, l [m], within a short time from t to $t + \Delta t$ as shown by Eq. (14).

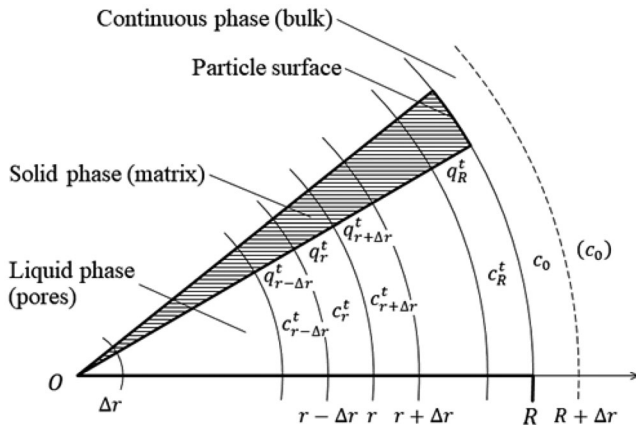


Figure 2. Schematic diagram of the concentric spherical shells we assumed in an adsorbent particle. This cross-section is represented by an arbitrary angle, and both liquid and solid phases were imaginarily drawn to each end.

$$C_l^{t+\Delta t} = C_l^t + \frac{D_L \Delta t}{\Delta l^2} (C_{l+\Delta l}^t - 2C_l^t + C_{l-\Delta l}^t) - \frac{u \Delta t}{\Delta l} (C_l^t - C_{l-\Delta l}^t) - \frac{3(1-\varepsilon)\varepsilon_p D'_{e,R} \Delta t}{R \varepsilon \Delta r} (C_l^t - C_{l,R}^t) \quad (14)$$

In Eq. (14), D_L is the axial dispersion coefficient [$\text{m}^2 \cdot \text{s}^{-1}$] and u is the average liquid velocity in the mobile phase [$\text{m} \cdot \text{s}^{-1}$]. The dimensionless concentrations C_l and $C_{l,R}$ [-] were the value in the mobile phase of the thin cross-section at distance l and that in the intraparticle liquid phase of the outermost thin-shell of the particles included in the same cross-section, respectively. The initial and boundary conditions applied to Eq. (14) are given by Eqs. (15)–(17).

$$C_l^0 = 0, \quad 0 \leq l \leq L \quad (15)$$

$$C_0^t = 1, \quad t \geq 0 \quad (16)$$

$$C_{L+\Delta L}^t = C_L^t, \quad t \geq 0 \quad (17)$$

To determine the $C_{l,R}$ in each cross-section, Eqs. (8) and (9) must be solved simultaneously with Eq. (14) under the initial and boundary conditions of Eqs. (10), (11) and (13) by substituting $C_r = C_{l,r}$ and $Q_r = Q_{l,r}$. Here, we applied another boundary condition regarding the concentration of the continuous phase (external particle), as shown by Eq. (18).

$$C_{l,R+\Delta r}^t = C_l^t, \quad t \geq 0 \quad (18)$$

According to the correlation for the Péclet number, Pe , by Rastegar and Gu (Rastegar and Gu 2017), we obtained $D_L = 1.18 \times 10^{-7} \text{ m}^2 \cdot \text{s}^{-1}$ ($\varepsilon \cdot Pe = 0.181$) by referring to our experimental conditions, and used this value in the calculation. The equations above were solved using the software Microsoft Visual Basic for Applications in Excel.

4. Results and discussion

4.1. Adsorption isotherm of a silica-based protein A medium

The adsorption isotherm of a silica-based protein A medium, M.S.Gel Protein A-D-50-1000AW, is shown in Figure 3. Experimental datapoints were approximated using the least square method in reference to Eq. (1) by using the solver in Microsoft Excel. The values for q_{bm} and K_d were $73.2 \text{ mg} \cdot \text{mL}^{-1}$ -packed-bed and $8.99 \times 10^{-3} \text{ mg} \cdot \text{mL}^{-1}$ -liquid, respectively. For reference, we also obtained the q_{bm} of $65.9 \text{ mg} \cdot \text{mL}^{-1}$ -packed-bed and K_d of $2.61 \times 10^{-2} \text{ mg} \cdot \text{mL}^{-1}$ -liquid for another commercial protein A medium, MabSelect Xtra. The values for this medium were comparable to those obtained by Hahn et al. (2005) and thus we concluded that the values for the silica-based protein A medium had been adequately measured.

As reported previously, the amount of coupled protein A in M.S.Gel Protein A-D-50-1000AW was more than $10.5 \text{ mg} \cdot \text{mL}^{-1}$ -packed-bed (Miyahara 2012). Based on this value and the above q_{bm} , the utmost capacity of protein A

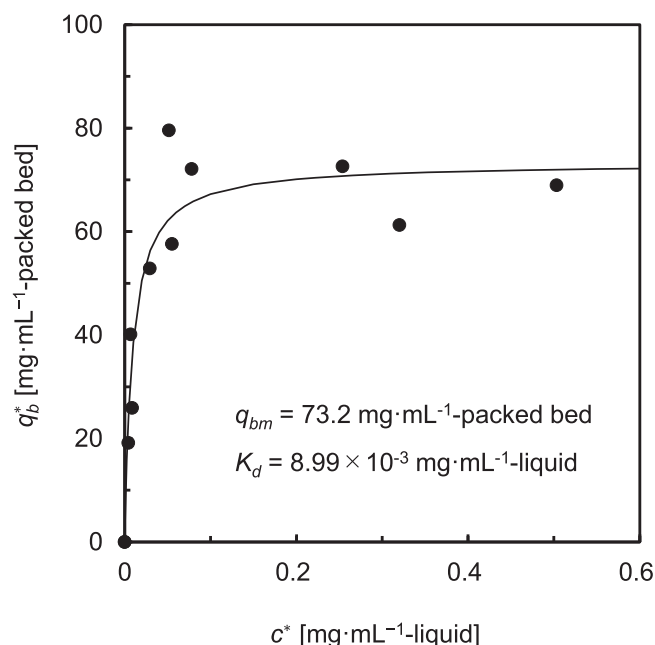


Figure 3. The adsorption isotherm of polyclonal hIgG for a silica-based protein A medium, M.S.Gel Protein A-D-50-1000AW. The data points were acquired from two independent experiments.

molecules in this medium was estimated to be 2.0 hIgG molecules per one protein A molecule. There are five IgG-binding domains in a Staphylococcal protein A molecule (Moks et al. 1986; Deis et al. 2015), but only two molecules of IgG are known to bind in solution (Langone et al. 1978; Yang et al. 2003). Given this fact, the coupled protein A molecules in this medium had likely bound with hIgG as free molecules would. However, the above K_d of $8.99 \times 10^{-3} \text{ mg} \cdot \text{mL}^{-1}$ -liquid corresponds to 61.6 nM, which is relatively higher than the reported values for free protein A molecules that range from 10 to 30 nM (Deis et al. 2015; Lindmark et al. 1983). We speculated that coupling to the matrix must have affected the spatial accessibility of hIgG, and when such an effect was combined with the molecular conformation of protein A, this must have altered both the association and the dissociation rates between hIgG and protein A.

4.2. Observation of the positional and temporal changes of adsorption ratio and determination of the apparent diffusivities in a silica-based protein A medium via CLSM

Figure 4 shows the adsorption ratios obtained from both CLSM and the numerical approximation (a)—included are the apparent diffusivities used in this approximation (b). In Figure 4(a), the datapoints are the experimental values determined from the fluorescence intensities in CLSM. The curves show the calculated values according to the numerical approximation. In this approximation, we assigned apparent diffusivities to the particle surface and also to the 6 interior subsections with an equal volume, and varied these using a trial-and-error approach. The fitted curves and apparent diffusivities were obtained after 35 trials. The constants and

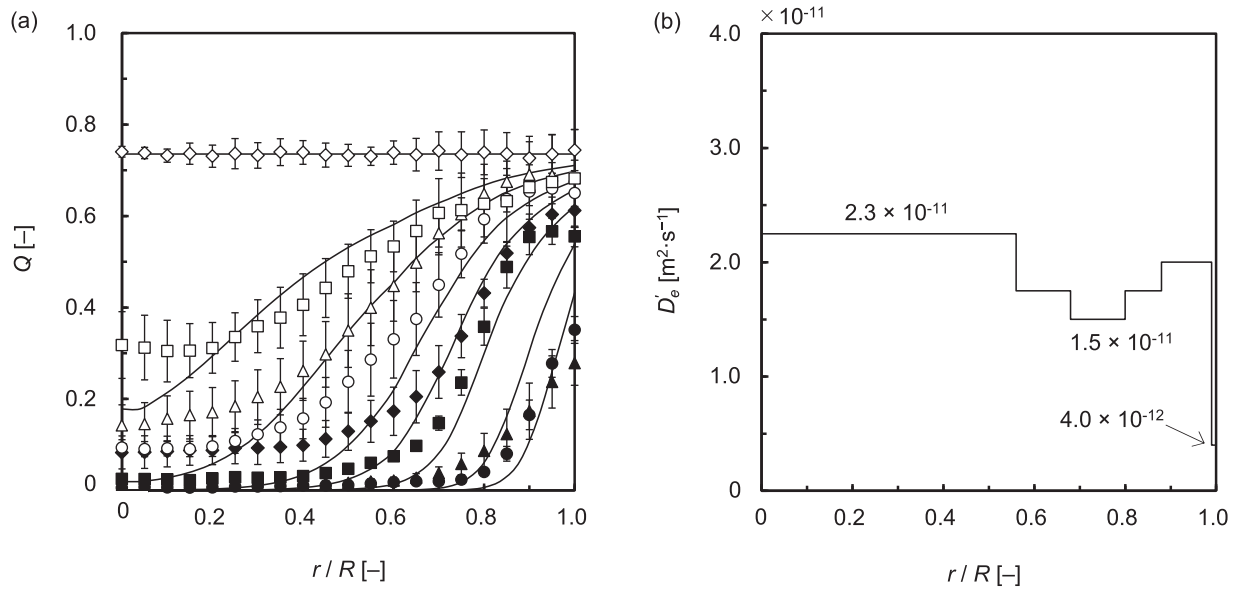


Figure 4. Temporal and positional changes in the adsorption ratios in single particles of silica-based protein A medium (a), and the apparent diffusivities used for the approximation curves (b). In (a), the points show the values determined from the fluorescence intensity observed in CLSM, and the approximation curves are our best result. Keys: closed circles, adsorption time of 0.5 h; closed triangles, 1 h; closed squares, 2 h; closed diamonds, 3 h; open circles, 4 h; open triangles, 6 h; open squares, 8 h; and, open diamonds, 28 h. The data points were determined from the fluorescence intensities of at least 3 particles for each adsorption time in a single set of batch adsorption experiment. The error bars indicate standard error of the mean.

Table 1. Constants and arbitrary values used in the numerical approximation.

hIgG concentration in continuous phase, c_0	$1.7 \times 10^{-4} \text{ mol}\cdot\text{m}^{-3}$ (0.025 mg·mL ⁻¹ -liquid)
Maximum adsorption amount per packed bed, q_{bm}	$5.0 \times 10^{-1} \text{ mol}\cdot\text{m}^{-3}$ (73 mg·mL ⁻¹ -packed bed)
Dissociation constant, K_d	$6.2 \times 10^{-5} \text{ mol}\cdot\text{m}^{-3}$ (9.0×10^{-3} mg·mL ⁻¹ -liquid)
Adsorption rate constant, k_a	$1.2 \times 10^2 \text{ m}^3\cdot\text{mol}^{-1}\cdot\text{s}^{-1a}$
Particle porosity, ϵ_p	0.53
Void fraction in packed bed, ϵ	0.4
Particle radius, R	$4.2 \times 10^{-5} \text{ m}$
Thickness of spherical shells, Δr	$8.4 \times 10^{-7} \text{ m}$
Length of short time, Δt	$5 \times 10^{-3} \text{ s}$

^aReported value (Hage et al. 1986.)

arbitrary values used in the numerical approximation are listed in Table 1.

The adsorption ratios that were obtained experimentally showed a rapid increase near the surface (i.e., $r/R > 0.8$) at the beginning of adsorption, but before reaching equilibrium the ratios of the inner portion (i.e., $r/R < 0.8$) started to increase. This type of adsorption behavior differs from the so-called “shrinking core” type, in which a clear border appears between the adsorbed and the unadsorbed sections and appears to shrink as time passes. Weinberg et al. compared the adsorption behaviors of monoclonal and polyclonal hIgGs in a cross-linked agarose-based protein A medium, CaptivA PriMAB (Weinberg et al. 2017). They reported two distinct shapes of the distribution of fluorescence intensity in CLSM wherein monoclonal IgG demonstrated curves with a fixed steep slope, but polyclonal IgG featured a sloping version that inclined over time. They attributed the difference to the presence of weaker and stronger binding species that compete for binding sites. Our results resembled the latter, which was understandable because we had used polyclonal hIgG in this research. Such an effect could have increased the experimental adsorption ratios near $r/R = 0$, which would have resulted in a somewhat higher apparent diffusivity in the numerical approximation.

Figure 4(b) shows the apparent diffusivities, D'_e , were $1.5\text{--}2.3 \times 10^{-11} \text{ m}^2\cdot\text{s}^{-1}$ for the interior subsections and $4.0 \times 10^{-12} \text{ m}^2\cdot\text{s}^{-1}$ for the surface of a particle. In the numerical approximation that determined these values, we had put emphasis on the range of $r/R \geq 0.5$, since 7/8 of the particle volume is in this range. We assumed that the apparent diffusivities, D'_e , of the interior of the particle might be variable depending on the distance from the center. When a fixed value of D'_e was applied—even if it was the volumetric mean of the values shown in Figure 4(b), it resulted in larger deviations in calculation curves comparing to those shown in Figure 4(a). This is shown in the supplementary information (Figure 1S), together with the case of too high or low values of D'_e .

For a comparison with other results, the values for the interior subsections were converted using Eq. (5) that showed an effective diffusivity, D_e , of $0.80\text{--}1.2 \times 10^{-11} \text{ m}^2\cdot\text{s}^{-1}$. Horstmann and Chase reported the effective diffusivities in Sepharose and Superose protein A media were within a range of from 0.12 to $1.1 \times 10^{-11} \text{ m}^2\cdot\text{s}^{-1}$ (Horstmann and Chase 1989). Similar values have been reported by other researchers: $4 \times 10^{-12} \text{ m}^2\cdot\text{s}^{-1}$ for MabSelect Xtra (Hahn et al. 2005), $5.3 \times 10^{-12} \text{ m}^2\cdot\text{s}^{-1}$ for CaptivA PriMAB (Weinberg et al. 2017), and 3.3×10^{-12}

and $1.7 \times 10^{-12} \text{ m}^2 \cdot \text{s}^{-1}$ for MabSelect SuRe and TOYOPEARL AF-rProtein A HC, respectively (da Silva et al. 2019). When comparing media consisting of cross-linked matrices, we found relatively high levels of effective diffusivity for the interior subsections of the silica-based medium. McCue et al. measured the effective diffusivities in both porous-glass- and agarose-based media and reported values of $1.0\text{--}2.0 \times 10^{-11}$ and $0.1\text{--}1.0 \times 10^{-11} \text{ m}^2 \cdot \text{s}^{-1}$, respectively (McCue et al. 2003). Our results for the interior subsections showed a similar range of effective diffusivity in porous-glass-based media, which verified these results as reasonable values for intraparticle mass-transfer properties.

We found the apparent diffusivity for the particle surface, $D'_{e,R}$, to be variable in proportion to the thickness, Δr , that separated the bulk of the continuous phase from the particle surface. Hence, the value of $4.0 \times 10^{-12} \text{ m}^2 \cdot \text{s}^{-1}$ that was obtained when $\Delta r = 0.84 \mu\text{m}$ was not comparable with values for the interior subsections, since the latter are independent of Δr . By using Eq. (6) we obtained a film mass-transfer coefficient, k_f , of $4.8 \times 10^{-6} \text{ m} \cdot \text{s}^{-1}$. The mass-transfer correlations for small particles in stirred vessels established by Calderbank and Moo-Young (Calderbank and Moo-Young 1961),

$$Sh = 0.13 Re^{3/4} Sc^{1/3} \quad (19)$$

and by Armenante and Kirwan (Armenante and Kirwan 1989),

$$Sh = 2 + 0.52 Re^{0.52} Sc^{1/3} \quad (20)$$

resulted in values for k_f of 2.0×10^{-6} and $1.1 \times 10^{-5} \text{ m} \cdot \text{s}^{-1}$, respectively. In these equations, Sh , Re , and Sc are dimensionless numbers [–], which Sherwood, Reynolds, and Schmidt, defined with Eqs. (21)–(23).

$$Sh = \frac{k_f(2R)}{D_m} \quad (21)$$

$$Re = \frac{E^{1/3}(2R)^{4/3}}{\nu} \quad (22)$$

$$Sc = \frac{\nu}{D_m} \quad (23)$$

In these equations, ν is the kinetic viscosity [$\text{m}^2 \cdot \text{s}^{-1}$], and E is the energy dissipation rate per unit of mass fluid [$\text{m}^2 \cdot \text{s}^{-3}$]. We applied $E = 2.8 \times 10^{-2} \text{ m}^2 \cdot \text{s}^{-3}$, which was obtained with the power number of 0.504 derived from an empirical equation by Nagata et al. (1957). The film mass-transfer coefficient derived from the apparent diffusivity at the particle surface, $D'_{e,R}$, was in the middle of the range of those from both correlations, for which the dissipation of turbulent kinetic energy was considered. In particular, the latter correlation has been adopted for protein adsorption, but it tends to give a relatively higher value since it was developed for highly agitated processes using a baffled vessel with a Rushton disk turbine (Armenante and Kirwan 1989; Weaver and Carta 1996). We emphasized the mass transfer due to free convection, instead of the turbulence in the surrounding fluid, when applying another correlation by

Calderbank and Moo-Young (Calderbank and Moo-Young 1961), as shown in Eq. (24).

$$Sh = 2 + 0.31 \left\{ \frac{(2R)^3 \Delta \rho}{\mu D_m} \right\}^{1/3} \quad (24)$$

In Eq. (24), $\Delta \rho$ is the difference in density between a particle and the continuous phase [$\text{kg} \cdot \text{m}^{-3}$], and μ is the viscosity [$\text{kg} \cdot \text{m}^{-1} \cdot \text{s}^{-1}$]. This correlation resulted in a similar value of $k_f = 4.9 \times 10^{-6} \text{ m} \cdot \text{s}^{-1}$. Thus, the apparent diffusivity of the particle surface appropriately reflected the properties of external mass transfer.

4.3. Application of the apparent diffusivities to numerical calculation of breakthrough curves

As described above, the apparent diffusivities derived from CLSM correspond to the mass-transfer properties of effective diffusivity and to an appropriate film mass-transfer coefficient, as determined in a conventional manner. By applying the apparent diffusivities shown in Figure 4(b), breakthrough curves were calculated and compared with an experimental curve (Figure 5). For this calculation, we applied the values of $u = 7.8 \times 10^{-4} \text{ m} \cdot \text{s}^{-1}$ and $\varepsilon = 0.65$ for the average liquid velocity in the mobile phase and its void fraction, respectively. These were identical to the experimental fix-bed adsorption. The thickness of the thin cross sections of the column, $\Delta l = 5 \times 10^{-4} \text{ m}$, was also applied.

The breakthrough curve of the dotted line, which was calculated with no adjustment to the apparent diffusivities, differed noticeably from the experimental results, particularly near the break point of $C = 0.1$. Generally, external mass transfer depends on the flow conditions around

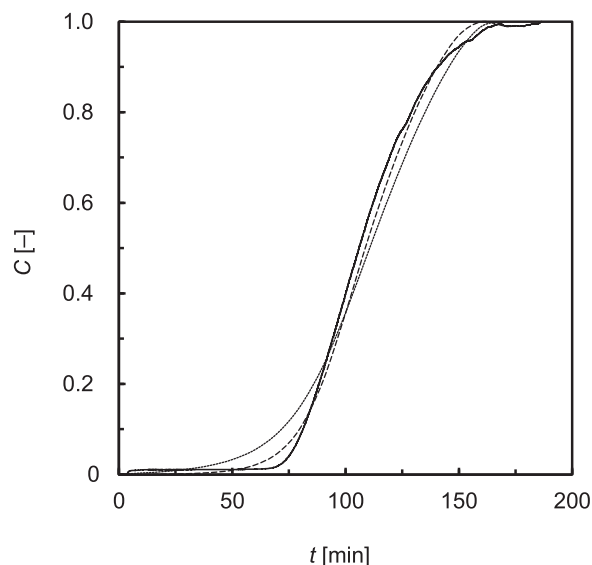


Figure 5. The breakthrough curve of hlgG experimentally obtained in a fixed-bed column of the silica-based protein A medium (solid line) and those calculated with the apparent diffusivities shown in Figure 4(b). The dashed line was calculated with the apparent diffusivity estimated from the correlation by Foo and Rice (Foo and Rice 1975), together with the values shown in Figure 4(b) for only the particle interior. The dotted line was done with all the values obtained in the batch adsorption. The experimentally-obtained breakthrough curve was of a single fixed-bed adsorption experiment.

adsorbent particles. We applied the value deduced from the correlation by Foo and Rice (Foo and Rice 1975) in order to establish the apparent diffusivity at the particle surface for the film mass-transfer coefficient in a packed bed.

$$Sh = 2 + 1.45 Re_p^{1/2} Sc^{1/3} \quad (25)$$

In Eq. (25), Re_p is the particle Reynolds number, which is defined by Eq. (26).

$$Re_p = \frac{(2R)\varepsilon u}{\nu} \quad (26)$$

The above correlation resulted in a relatively higher $D'_{e,R}$ of $6.6 \times 10^{-12} \text{ m}^2 \cdot \text{s}^{-1}$ by comparison with our batch-experiment value of $4.0 \times 10^{-12} \text{ m}^2 \cdot \text{s}^{-1}$. The calculated breakthrough curve continued to show a slight difference with the experimental results, although it might be acceptable as a rough approximation. The dynamic binding capacities at the 10% break point were $31.8 \text{ mg} \cdot \text{mL}^{-1}$ (calculation with the correlation by Foo and Rice) and $32.2 \text{ mg} \cdot \text{mL}^{-1}$ (experiment). Thus, the apparent diffusivities, except for the particle surface as determined above, were applicable to predict the breakthrough curves and dynamic binding capacities. When a too high or low values of D'_e was applied, it resulted in a larger deviation in calculation curves (Figure 2S).

Though we loaded unlabeled human IgG, the experimentally obtained breakthrough curve was acceptably predicted using the apparent diffusivities that were determined based on the adsorption of FITC-labeled human IgG. This suggests a negligible effect of fluorescein labeling on the adsorption of IgG to a protein A medium. The F/P ratio of the FITC-hIgG we used was 2.4 and this seems sufficiently small for hIgG to interfere the adsorption in a protein A medium. However, conjugating a fluorescent label with an adsorbate can sometimes be problematic when attempting to observe the intraparticle adsorption behaviors via CLSM. Teske et al. compared unlabeled lysozymes and lysozymes conjugated with different fluorescent labels and showed the latter

version had a shorter retention in a cation exchange column of SP Sepharose Fast Flow, and this result was consistent with the difference in net charge (Teske et al. 2005). On the other hand, Corbett et al. mentioned that fluorescent labels did not substantially affect the interaction between the anion exchange medium Fractogel TMAE HiCap (M) and bovine serum albumin or thyroglobulin (Corbett et al. 2013). As shown in these cases of ion exchangers, the large molecular mass of an adsorbate likely moderates labeling effects.

4.4. Light attenuation via the particle matrix of a silica-based protein A medium

From the results shown above, the use of CLSM for the quantitative analysis of mass transfer appears practical also for protein A media. However, Susanto et al. showed that the matrix of an adsorbent particle was likely to cause an attenuation of light depending on the path length, which led to an uneven measurement of the fluorescence intensity (Susanto et al. 2007). Since the thickness of a spherical matrix increases from the perimeter to the center when a particle is scanned horizontally, the light path length varies in the radial direction. In order to clarify the effects of this variation on the fluorescence intensity, the silica-based medium was examined via CLSM after soaking overnight in a $1 \text{ mg} \cdot \text{mL}^{-1}$ fluorescein solution, which fluoresced itself when excited. Figure 6(a) shows the fluorescence image of a particle in the silica-based medium in the fluorescein solution, and the fluorescence intensities along the line of a region of interest (ROI) are plotted in Figure 6(b). A solution of $1 \text{ mg} \cdot \text{mL}^{-1}$ of fluorescein provided a negative image of the particle, and its fluorescence intensities were independent of the distance from the center. This suggests that the effect of matrix thickness on fluorescence intensity was either absent or negligible in the silica-based medium, which suggests that the adsorption amounts converted from the fluorescence intensities obtained by CLSM are valid.

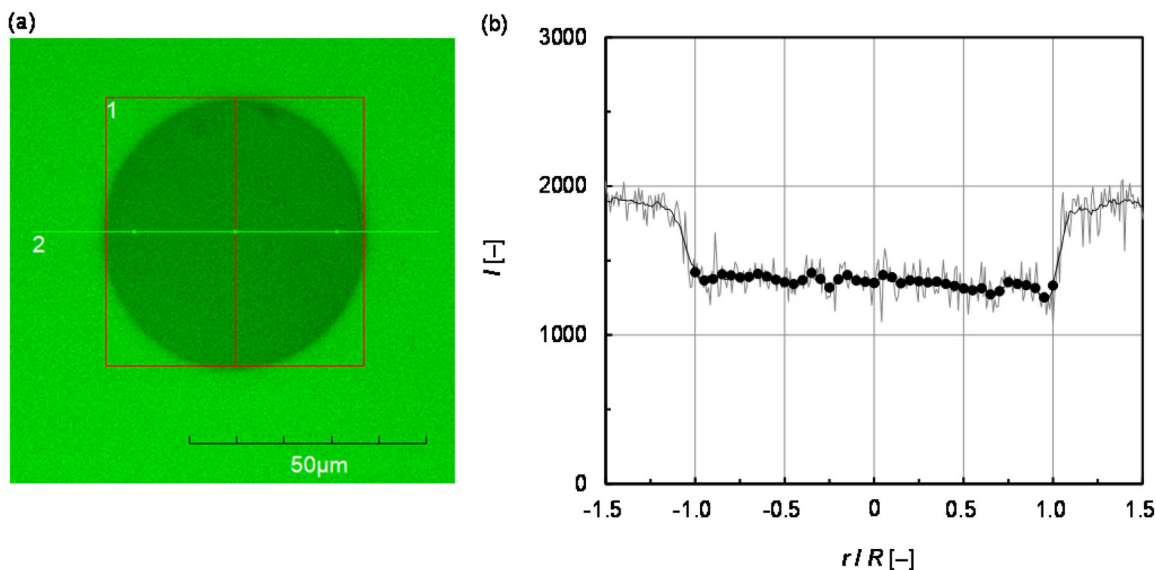


Figure 6. The fluorescence image of a representative particle of the silica-based protein A medium soaked overnight in a $1 \text{ mg} \cdot \text{mL}^{-1}$ fluorescein solution (a) and the distribution of fluorescence intensities of this particle along the line of ROI shown in (a) passing through the particle center (b).

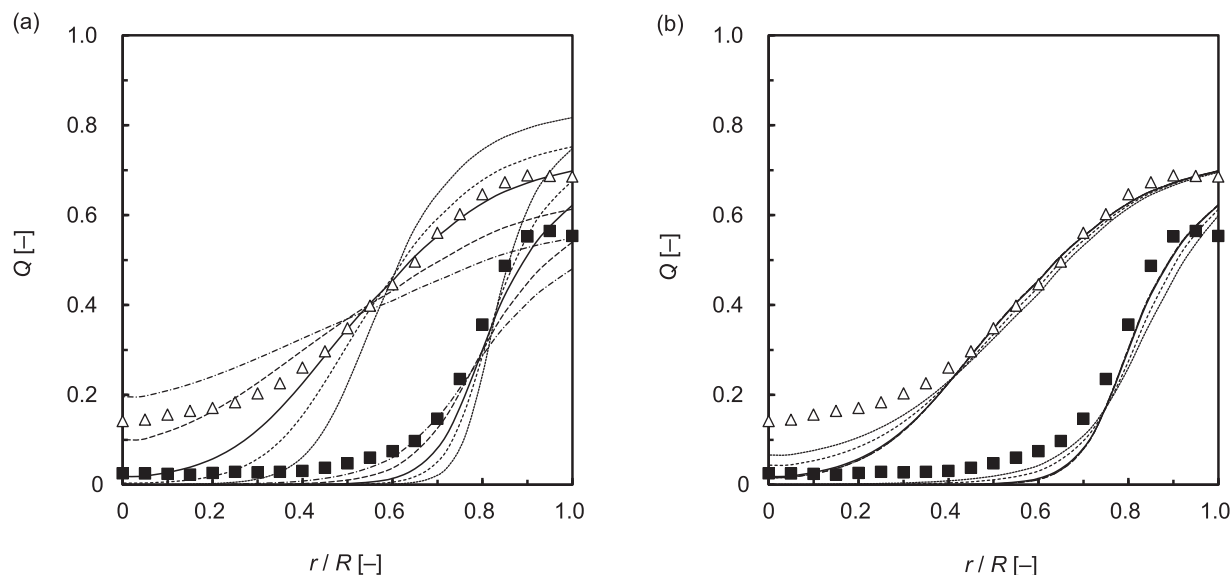


Figure 7. The effect of K_d (a) and k_a (b) on the shape of the curve of adsorption ratios. The experimental data points were extracted from Figure 4(a). Lines in (a): solid, $\times 1$ of the experimental value; dotted, $\times 1/4$; densely dashed, $\times 1/2$; dashed, $\times 2$; and, chain, $\times 4$. Lines in (b): solid, $\times 1$ of the literature value [34]; dotted, $\times 1/20$; densely dashed, $\times 1/10$; dashed, $\times 10$; and, chain, $\times 20$.

4.5. Effects of K_d and k_a

In this study, we did not assume an instantaneous equilibration at the adsorption sites, and accordingly the adsorption kinetics were incorporated in the partial differential Eqs. (3) and (4) as well as Eqs. (8) and (9), which apply to the free or adsorbed hIgGs, respectively. The dissociation constant, K_d , was experimentally determined, but for the association rate constant, k_a , we relied on a reported value of $120 \text{ mol}^{-1} \cdot \text{m}^3 \cdot \text{s}^{-1}$ (Hage et al. 1986). Hence, we noted the effects that these values exerted on the calculated curves.

As shown in Figure 7(a,b), the value of K_d drastically changed the shape of the curve even if the variation was smaller or larger than only 2-fold, but that of k_a did not significantly affect the shape even when the variation was as much as 20-fold. This implies that the difference in rates of association and dissociation at adsorption sites rapidly become small, and thus the partitioning between the liquid and the solid phases was effective for the curve shape. Therefore, if there was diversity in the value of K_d , like that of polyclonal hIgG as mentioned in the previous section, the fluorescence-intensity distribution would show a composite shape.

5. Conclusions

In this study, we analyzed the mass transfer of polyclonal hIgG in a silica-based protein A medium. The positional and temporal changes in the batch adsorption amount were monitored via CLSM, and the adsorption behavior was numerically approximated using a simple theoretical model to obtain mass-transfer properties in single particles. In this approximation, we adopted a trial-and-error approach and determined the apparent diffusivities for both external and intraparticle mass transfer. Though the uncertainty in this approach must be eliminated or further reduced, the resultant values showed good agreement with the reported ones

and also were applicable to predicting a breakthrough curve. The most important advantage in this microscopic analysis is that we are now able to concurrently determine both the external and intraparticle mass-transfer properties based on the direct observation of adsorption behavior. In a subsequent study, we will apply this method to another type of protein A media and use it to clarify the mass-transfer properties.

Acknowledgements

The authors would like to express our sincere gratitude to Mr. Hiroyoshi Miyahara and Mr. Ryou Nakashima of AGC Si-Tech Co., Ltd. for their kind support and valuable discussions. We are thankful to the students who made dedicated efforts to this research and brought us precious experiences: Mr. Takuya Nishiyama, Mr. Toru Yoshikawa, Ms. Maya Hayashi, Mr. Yusuke Haruna, and Mr. Keita Hirose.

References

- Armenante PM, Kirwan DJ. 1989. Mass transfer to microparticles in agitated systems. *Chem Eng Sci.* 44:2781–2796.
- Bowes BD, Lenhoff AM. 2011. Protein adsorption and transport in dextran-modified ion-exchange media. II. Intraparticle uptake and column breakthrough. *J Chromatogr A.* 1218:4698–4708.
- Calderbank PH, Moo-Young MB. 1961. The continuous phase heat and mass-transfer properties of dispersions. *Chem Eng Sci.* 16:39–54.
- Chase HA. 1984. Prediction of the performance of preparative affinity chromatography. *J Chromatogr.* 297:179–202.
- Corbett R, Carta G, Iskra T, Gallo C, Godavarti R, Salm JR. 2013. Structure and protein adsorption mechanisms of clean and fouled tentacle-type anion exchangers used in a monoclonal antibody polishing step. *J Chromatogr A.* 1278:116–125.
- da Silva GFL, Plewka J, Tscheließnig R, Lichtenegger H, Jungbauer A, Dias-Cabral ACM. 2019. Antibody binding heterogeneity of protein A resins. *Biotechnol J.* 14:1800632.
- Deis LN, Wu Q, Wang Y, Qi Y, Daniels KG, Zhou P, Oas TG. 2015. Suppression of conformational heterogeneity at a protein–protein interface. *Proc Natl Acad Sci USA.* 112:9028–9033.

- Foo SC, Rice RG. 1975. On the prediction of ultimate separation in parametric pumps. *AIChE J.* 21:1149–1158.
- Hage DS, Walters RR, Hethcote HW. 1986. Split-peak affinity chromatographic studies of the immobilization-dependent adsorption kinetics of protein A. *Anal Chem.* 58:274–279.
- Hahn R, Bauerhansl P, Shimahara K, Wizniewski C, Tscheliessnig A, Jungbauer A. 2005. Comparison of protein A affinity sorbents. II. Mass transfer properties. *J Chromatogr A.* 1093:98–110.
- Horstmann BJ, Chase HA. 1989. Modeling the affinity adsorption of immunoglobulin-G to protein-A immobilized to agarose matrices. *Chem Eng Res Des.* 67:243–254.
- Hubbuch J, Linden T, Knieps E, Thömmes J, Kula M-R. 2002. Dynamics of protein uptake within the adsorbent particle during packed bed chromatography. *Biotechnol Bioeng.* 80:359–368.
- Jøssang T, Feder J, Rosenqvist E. 1988. Photon correlation spectroscopy of human IgG. *J Protein Chem.* 7:165–171.
- Kasche V, de Boer M, Lazo C, Gad M. 2003. Direct observation of intraparticle equilibration and the rate-limiting step in adsorption of proteins in chromatographic adsorbents with confocal laser scanning microscopy. *J Chromatogr B.* 790:115–129.
- Katoh S, Imada M, Takeda N, Katsuda T, Miyahara H, Inoue M, Nakamura S. 2007. Optimization of silica-based media for antibody purification by protein A affinity chromatography. *J Chromatogr A.* 1161:36–40.
- Kim H-B, Hayashi M, Nakatani K, Kitamura N, Sasaki K, Hotta J-I, Masuhara H. 1996. In situ measurements of ion-exchange processes in single polymer particles: laser trapping microspectroscopy and confocal fluorescence microspectroscopy. *Anal Chem.* 68:409–414.
- Langmuir I. 1916. The constitution and fundamental properties of solids and liquids. Part I. Solids. *J Am Chem Soc.* 38:2221–2295.
- Langone JJ, Boyle MDP, Borsos T. 1978. Studies on the interaction between protein A and immunoglobulin G. I. Effect of protein A on the functional activity of IgG. *J Immunol.* 121:327–332.
- LeVan MD, Carta G, Carmen M. 1999. Adsorption and ion exchange. In: Perry RH, Green DW, Maloney JO, editors. *Perry's chemical engineers' handbook*. 7th ed., Section 16. New York: McGraw Hill.
- Linden T, Ljunglöf A, Kula M-R, Thömmes J. 1999. Visualizing two-component protein diffusion in porous adsorbents by confocal scanning laser microscopy. *Biotechnol Bioeng.* 65:622–630.
- Linden T, Ljunglöf A, Hagel L, Kula M-R, Thömmes J. 2002. Visualizing patterns of protein uptake to porous media using confocal scanning laser microscopy. *Sep Sci Technol.* 37:1–32.
- Lindmark R, Thorén-Tolling K, Sjöquist J. 1983. Binding of immunoglobulins to protein A and immunoglobulin levels in mammalian sera. *J Immunol Methods.* 62:1–13.
- Ljunglöf A, Thömmes J. 1998. Visualising intraparticle protein transport in porous adsorbents by confocal microscopy. *J Chromatogr A.* 813:387–395.
- Ljunglöf A, Hjorth R. 1996. Confocal microscopy as a tool for studying protein adsorption to chromatographic matrices. *J Chromatogr A.* 743:75–83.
- McCue JT, Kemp G, Low D, Quiñones-García I. 2003. Evaluation of protein-A chromatography media. *J Chromatogr A.* 989:139–153.
- Miyahara H, Nakashima R, Inoue M, Katsuda T, Yamaji H, Katoh S. 2012. Optimization and performance of silica-based media for industrial-scale antibody purification. *Chem Eng Technol.* 35:157–160.
- Moks T, Abrahamsén L, Nilsson B, Hellman U, Sjöquist J, Uhlén M. 1986. Staphylococcal protein A consists of Five IgG-binding domains. *Eur J Biochem.* 156:637–643.
- Nagata S, Yamamoto K, Yokoyama T, Shiga S. 1957. Empirical equations for the power requirement of mixing impellers, having a wide range of applicability. *Chem Eng.* 21:708–715.
- Rastegar SO, Gu T. 2017. Empirical correlations for axial dispersion coefficient and Peclet number in fixed-bed columns. *J Chromatogr A.* 1490:133–137.
- Schröder M, von Lieres E, Hubbuch J. 2006. Direct quantification of intraparticle protein diffusion in chromatographic media. *J Phys Chem B.* 110:1429–1436.
- Sheth B. 2009. Characterisation of chromatography adsorbents for antibody bioprocessing [master thesis]. London: University College London.
- Stone MC, Carta G. 2007. Patterns of protein adsorption in chromatographic particles visualized by optical microscopy. *J Chromatogr A.* 1160:206–214.
- Subramanian A, Van Cott KE, Milbrath DS, Velandier WH. 1994. Role of local antibody density effects on immunosorbent efficiency. *J Chromatogr A.* 672:11–24.
- Susanto A, Herrmann T, von Lieres E, Hubbuch J. 2007. Investigation of pore diffusion hindrance of monoclonal antibody in hydrophobic interaction chromatography using confocal laser scanning microscopy. *J Chromatogr A.* 1149:178–188.
- Teske CA, Schroeder M, Simon R, Hubbuch J. 2005. Protein-labeling effects in confocal laser scanning microscopy. *J Phys Chem B.* 109:13811–13817.
- Thermo Fisher Scientific Inc. 2011. Calculate dye: protein (F/P) molar ratios. [accessed 2022 Jan 4]. <https://tools.thermofisher.com/content/sfs/brochures/TR0031-Calc-FP-ratios.pdf>.
- Tscheliessnig A, Hahn R, Jungbauer A. 2005. In situ determination of adsorption kinetics of proteins in a finite bath. *J Chromatogr A.* 1069:23–30.
- Weaver JLE, Carta G. 1996. Protein adsorption on cation exchangers: comparison of macroporous and gel-composite media. *Biotechnol Prog.* 12:342–355.
- Weinberg J, Zhang S, Crews G, Healy E, Carta G, Przybycien T. 2017. Polyclonal and monoclonal IgG binding on protein A resins—evidence of competitive binding effects. *Biotechnol Bioeng.* 114:1803–1812.
- Yamamoto S, Nakanishi K, Matsuno R. 1988. Ion-exchange chromatography of proteins. New York: Marcel Dekker.
- Yang L, Biswas ME, Chen P. 2003. Study of binding between protein A and immunoglobulin G using a surface tension probe. *Biophys J.* 84:509–522.
- Zhou X-P, Li W, Shi Q-H, Sun Y. 2006. Analysis of mass transport models for protein adsorption to cation exchanger by visualization with confocal laser scanning microscopy. *J Chromatogr A.* 1103:110–117.

Nomenclature

Roman symbols

c	Concentration of free IgG [$\text{mol}\cdot\text{m}^{-3}$]
c^*	Equilibrium free-IgG concentration [$\text{mg}\cdot\text{mL}^{-1}$ -liquid]
c_0	Concentration of IgG in the continuous phase [$\text{mol}\cdot\text{m}^{-3}$]
C	Dimensionless concentration ($= c/c_0$)
D_e	Effective diffusivity [$\text{m}^2\cdot\text{s}^{-1}$]
D_e^f	Apparent diffusivity [$\text{m}^2\cdot\text{s}^{-1}$]
$D_{e,R}$	Apparent diffusivity of the particle surface [$\text{m}^2\cdot\text{s}^{-1}$]
D_L	Axial dispersion coefficient [$\text{m}^2\cdot\text{s}^{-1}$]
D_m	Molecular diffusivity [$\text{m}^2\cdot\text{s}^{-1}$]
E	Energy dissipation rate per unit of mass fluid [$\text{m}^2\cdot\text{s}^{-3}$]
I_r^*	Fluorescence intensity in equilibrium at distance r (arbitrary unit)
k_a	Association rate constant [$\text{m}^3\cdot\text{mol}^{-1}\cdot\text{s}^{-1}$]
K_d	Dissociation constant between protein A and IgG [$\text{mg}\cdot\text{mL}^{-1}$ -liquid or $\text{mol}\cdot\text{m}^{-3}$]
k_f	Film mass-transfer coefficient [$\text{m}\cdot\text{s}^{-1}$]
l	Distance from the column inlet [m]
L	Axial length of a column [m]
Pe	Péclet number [–]
q	Amount of adsorbed IgG per pore volume [$\text{mol}\cdot\text{m}^{-3}$]
q_b	Amount of adsorbed IgG per packed-bed volume [$\text{mg}\cdot\text{mL}^{-1}$ -packed-bed]
q_{bm}	Maximum amount of adsorbed IgG per packed-bed volume [$\text{mg}\cdot\text{mL}^{-1}$ -packed-bed]

q_b^*	Equilibrium adsorbed amount of IgG per packed-bed volume [mg·mL ⁻¹ -packed-bed]	Δl	Thickness of thin cross-sections of a column [m]
q_m	Maximum amount of adsorbed IgG per pore volume [mol·m ⁻³]	Δr	Thickness of concentric spherical shells assumed in a particle [m]
Q	Adsorption ratio ($= q/q_m$)	Δt	Short time [s]
r	Distance from the particle center [m]	$\Delta \rho$	Difference in density between a particle and the continuous phase [kg·m ⁻³]
R	Particle radius [m]	ε	Void fraction of the packed bed
Re	Reynolds number [-]	ε_p	Porosity of adsorbent particles [-]
Re_p	Particle Reynolds number	μ	Viscosity [kg·m ⁻¹ ·s ⁻¹]
Sh	Sherwood number [-]	τ	Tortuosity factor [-]
Sc	Schmidt number [-]	ν	Kinetic viscosity [m ² ·s ⁻¹]
u	Average liquid velocity in the mobile phase [m·s ⁻¹]		

Greek symbols

α	Conversion factor [mg·mL ⁻¹ -packed-bed]
δ	Film thickness [m]

Subscripts

i	Index of the datapoints numbered from the center to the outer surface
-----	---